



Since January 2020 Elsevier has created a COVID-19 resource centre with free information in English and Mandarin on the novel coronavirus COVID-19. The COVID-19 resource centre is hosted on Elsevier Connect, the company's public news and information website.

Elsevier hereby grants permission to make all its COVID-19-related research that is available on the COVID-19 resource centre - including this research content - immediately available in PubMed Central and other publicly funded repositories, such as the WHO COVID database with rights for unrestricted research re-use and analyses in any form or by any means with acknowledgement of the original source. These permissions are granted for free by Elsevier for as long as the COVID-19 resource centre remains active.

# A modified porous silicon microparticle potentiates protective systemic and mucosal immunity for SARS-CoV-2 subunit vaccine



AWADALKAREEM ADAM<sup>#</sup>, QING SHI<sup>#</sup>, BINBIN WANG, JING ZOU, JUNHUA MAI, SAMANTHA R. OSMAN, WENZHE WU, XUPING XIE, PATRICIA V AGUILAR, XIAOYONG BAO, PEI-YONG SHI, HAIFA SHEN, and TIAN WANG

GALVESTON, AND HOUSTON, TEXAS

**Development of optimal SARS-CoV-2 vaccines to induce potent, long-lasting immunity and provide cross-reactive protection against emerging variants remains a high priority. Here, we report that a modified porous silicon microparticle (mPSM) adjuvant to SARS-CoV-2 receptor-binding domain (RBD) vaccine activated dendritic cells and generated more potent and durable systemic humoral and type 1 helper T (Th) cell-mediated immune responses than alum-formulated RBD following parenteral vaccination, and protected mice from SARS-CoV-2 and Beta variant challenge. Notably, mPSM facilitated the uptake of SARS-CoV-2 RBD antigens by nasal and airway epithelial cells. Parenteral and intranasal prime and boost vaccinations with mPSM-RBD elicited stronger lung resident T and B cells and IgA responses compared to parenteral vaccination alone, which led to markedly diminished viral loads and inflammation in the lung following SARS-CoV-2 Delta variant challenge. Overall, our results suggest that mPSM is effective adjuvant for SARS-CoV-2 subunit vaccine in both systemic and mucosal vaccinations. (Translational Research 2022; 249:13–27)**

**Abbreviations:** mPSM = modified porous silicon microparticle; COVID-19 = coronavirus disease 2019; RBD = receptor-binding domain; SARS-CoV-2 = severe acute respiratory syndrome coronavirus 2;  $\beta$ -COV = Betacoronavirus; E = envelope; M = membrane; N = nucleocapsid; hACE2 = human angiotensin-converting enzyme 2; NAb = neutralizing antibodies; DC = dendritic cell; Th1 = T helper 1; CpG = Cytosine guanosine dinucleotide; cGAMP = cyclic GAMP; BM = bone marrow; i.p. = intraperitoneally; i.d. = intradermally; i.m. = or intramuscularly; TMB = Tetramethylbenzidine; PBS-T = Phosphate-buffered saline containing Tween-20; BAL = bronchoalveolar lavage; HRP = horseradish peroxidase; ELISA = Enzyme-linked immunosorbent assay; ELISPOT = Enzyme-linked immune absorbent spot; SFC = spot-forming cells; ICS = intracellular cytokine staining; MOI = multiplicity of infection; APC = antigen presenting cells; MBC = memory B cell; ASC = antibody secreting cells; PRNT = plaque reduction neutralization test; SAEC = small airway epithelial cells; NALT = nasal-associated lymphoid tissue; ADE = antibody-dependent Enhancement; Q-PCR = quantitative PCR

<sup>#</sup>Equal contribution.

From the Department of Microbiology & Immunology, University of Texas Medical Branch, Galveston, Texas; Department of Nanomedicine, Houston Methodist Academic Institute, Houston, Texas; Department of Biochemistry & Molecular Biology, University of Texas Medical Branch, Galveston, Texas; Department of Pediatrics, The University of Texas Medical Branch, Galveston, Texas; Department of Pathology, University of Texas Medical Branch, Galveston, Texas; Sealy Institute for Vaccine Sciences, University of Texas Medical Branch, Galveston, Texas; Institute for Human Infections and Immunity, University of Texas Medical Branch, Galveston, Texas; Innovative Therapeutic Program, Houston Methodist Cancer Center, Houston, Texas; ImmunoQ Therapeutics, Houston, Texas.

Submitted for Publication March 21, 2022; revision submitted May 30, 2022; Accepted for Publication June 2, 2022.

Reprint requests: Tian Wang, Department of Microbiology & Immunology, University of Texas Medical Branch, Galveston, TX, 77555, USA E-mail address: [haifashen@gmail.com](mailto:haifashen@gmail.com).

1931-5244/\$ - see front matter

© 2022 Elsevier Inc. All rights reserved.

<https://doi.org/10.1016/j.trsl.2022.06.004>

**At A Glance Commentary**

Adam A, et al.

**Background**

Development of optimal SARS-CoV-2 vaccines to induce potent, long-lasting immunity and provide cross-reactive protection against emerging variants remains a high priority.

**Translational Significance**

A modified porous silicon microparticle (mPSM) adjuvant to SARS-CoV-2 receptor-binding domain (RBD) vaccine generated potent and durable systemic humoral and type 1 helper T (Th) cell-mediated immunity following parenteral vaccination. mPSM also facilitated mucosal uptake of SARS-CoV-2 RBD antigens. Parenteral and intranasal prime and boost vaccinations with mPSM-RBD elicited strong mucosal immune responses and protected mice from SARS-CoV-2 variant challenge. These results suggest that mPSM is effective adjuvant for SARS-CoV-2 subunit vaccine in both systemic and mucosal vaccinations.

**INTRODUCTION**

The coronavirus disease 2019 (COVID-19) pandemic, which was caused by severe acute respiratory syndrome coronavirus 2 (SARS-CoV-2), has made a devastating impact on global public health and economy over the past 2 years. SARS-CoV-2 belongs to the genus *Betacoronavirus* ( $\beta$ -COV) of the family *Coronaviridae* and contains a single-stranded positive-sense RNA genome. The genome encodes structural proteins (spike [S], envelope [E], membrane [M] and nucleocapsid [N]), nonstructural proteins (nsp1-nsp16), and several accessory proteins.<sup>1</sup> The S protein is the major virus surface glycoprotein that engages the interaction with human angiotensin-converting enzyme 2 (hACE2) through its receptor-binding domain (RBD) and facilitates virus entry into target cells. Both the S protein and the RBD can elicit highly potent neutralizing antibodies (NAbs) and contain major T cell epitopes, thus have been the main targets for vaccine development.<sup>2-4</sup>

In response to the pandemic, many vaccine platforms have been rapidly developed and tested to enable production of effective vaccines against SARS-CoV-2 infection. This includes inactivated vaccines, subunit vaccines, DNA vaccines, mRNA vaccines, viral vectored vaccines, and live-attenuated vaccines.<sup>1,5-9</sup> Currently, 3 vaccines have been granted emergency use

authorization (EUA) from the FDA. However, the increasing rate of emergence of variants with enhanced viral transmission and disease severity in COVID-19 patients,<sup>10,11</sup> potential concerns of “vaccine-induced disease enhancement”<sup>12</sup> and risk of antibody-dependent enhancement due to waning immunity after vaccination<sup>13</sup> have together posed additional challenges for the global vaccine efficiency efforts. It is clear that continuous efforts toward optimizing existing vaccine platforms and development of more effective novel vaccines are needed. Although intranasal immunization can lead to the induction of antigen-specific immunity in both the mucosal and systemic immune compartments,<sup>14</sup> most SARS-CoV-2 vaccines, in particular the subunit vaccines are limited to parenteral injection. One of the challenges is that soluble antigens delivered to the nasal passages do not breach the epithelial barrier but instead were transported by microfold cells.<sup>15</sup>

Porous silicon microparticle (PSM) can serve as a carrier and a reservoir to maintain sustained release of proteins and peptide antigens inside dendritic cell (DC) s.<sup>16</sup> PSMs were previously shown to have protective effects as an adjuvant for cancer vaccines to stimulate T helper 1 (Th1) immunity. The modified (m)PSM, prepared by loading the TLR9 ligand cytosine guanosine dinucleotide (CpG) and STING agonist 2'-3'-cyclic GAMP (cGAMP)- to PSMs, can elicit higher levels of IFN I and inflammatory cytokines in DCs than PSM, and induces strong anti-tumor Th1 type immunity.<sup>17</sup> In this study, we evaluated the immunogenicity and safety of mPSM adjuvant with SARS-CoV-2 S protein RBD subunit vaccine (mPSM-RBD) following parenteral and mucosal vaccinations in mice and assessed the protective efficacy of mPSM-RBD vaccine against SARS-CoV-2 variants challenge.

**MATERIALS AND METHODS**

**Vaccine preparation.** To express and purify the RBD protein, the amino acid residues of 319–541 of SARS-CoV-2 S protein were cloned into the lentivirus vector, pCDH-CMV-MCS-EF1 $\alpha$ -RFP (System Biosciences). To facilitate the secretion and purification of the protein, the first 19 residues of the S protein and a hexahistidine (6xHis) tag were fused at the N-terminal as a secretion signal and the C-terminal respectively. The vector was then packaged into lentivirus to transduce 293FT cells. RBD protein was purified from culture supernatant using His-Trap Excel nickel column (Cytiva). In all experiments, mPSM was prepared to include 1  $\mu$ g CpG ODN (Invivogen) 1826 and 0.5  $\mu$ g cGAMP (Invivogen) in PSM ( $6 \times 10^7$  particles, equivalent to 12  $\mu$ g) as described previously.<sup>16,17</sup> Twenty-

five microliter of Inject Alum (ThermoFisher) was mixed with RBD protein 30 min before inoculation.

**Viruses.** SARS-CoV-2 Beta variant, and Delta variant were obtained from the World Reference Center for Emerging Viruses and Arboviruses (WRCEVA) at the University of Texas Medical Branch (UTMB) and were amplified twice in Vero E6 cells. The generation of the mouse-adapted SARS-CoV-2 strain CMA4 was described in a recent study.<sup>18</sup> The virus stocks for experiments were sequenced to ensure no undesired mutations in the S genes during the amplification in Vero E6 cells.

**Mice.** 6-week-old BALB/c mice, C57BL/6 mice, and K18 hACE2 mice (stock #034860) were purchased from Jackson Lab. For vaccination, mice were inoculated intraperitoneally (i.p.), intradermally (i.d.), or intramuscularly (i.m.) with 5–25  $\mu$ g RBD conjugated with mPSM or Alum on days 0, and 14 or 21. In some experiments, mice were i.p. primed on day 0 and boosted with the same dose on day 21 via intranasal (i.n.) inoculation. Vaccinated mice were challenged with  $1 \times 10^4$  PFU of SARS-CoV-2 CMA4, or Delta variant, or  $4 \times 10^3$  PFU SARS-CoV-2 Beta variant. Infected mice were monitored twice daily for signs of morbidity. On days 2 or 4 postinfection, mice were euthanized for tissue collection. All animal experiments were approved by the Animal Care and Use Committees at UTMB and Houston Methodist Academic Institute, respectively.

**In vitro DC maturation assay.** Bone marrow (BM)-derived DCs were generated as described previously [16]. Briefly, BM cells isolated from BALB/c mice were cultured for 6 days in medium supplemented with granulocyte-macrophage colony-stimulating factor (GM-CSF) and IL-4 (Peprotech) to generate DCs. DCs were then treated with RBD alone or together with alum or mPSM at 37°C for 24 h. Cells were harvested and stained with antibodies for cell surface markers, including CD80 or CD86 antibodies (BioLegend), and acquired by a BD LSR II flow cytometer (BD Biosciences). Data were analyzed using FlowJo software (BD Biosciences).

**Antibody ELISA.** Plates were coated with 1  $\mu$ g/mL of purified SARS-CoV-2 RBD protein overnight at 4°C. Plates were blocked with 1% BSA for 45 min at 37°C. Diluted serum samples were added and incubated for 2 h at room temperature. This will be followed by a 1 h incubation with biotinylated HRP conjugated goat anti-mouse IgG subtype antibodies (Southern Biotech). 3,3',5,5' tetramethylbenzidine (TMB, BD Biosciences) were added to the well for 15 min and reactions were stopped by sulfuric acid. Absorbance at 450 nm and 570 nm were read and the absorbance at 570 nm was subtracted from the absorbance at 450 nm. Binding endpoint titers were determined using a cutoff value

which is negative control+10x SD. In some experiments, ELISA plates were coated with 250 ng/well recombinant SARS-2 RBD protein (RayBiotech, USA) for overnight at 4°C. The plates were washed twice with phosphate-buffered saline, containing 0.05% Tween-20 (PBS-T) and then blocked with 8% FBS for 1.5 h. Sera or bronchoalveolar lavage (BAL) were diluted 1:40–1:100 or undiluted in blocking buffer and were added for 1 h at 37°C. Plates were washed 5 times with PBS-T. Goat anti-mouse IgG (Sigma, MO, USA), goat anti-mouse IgG1, Goat anti-mouse IgG2a, or goat anti-mouse IgG2b (Southern Biotech) coupled to alkaline phosphatase was added at a 1:1000–1:2000 dilutions for 1 h at 37°C. Color was developed with *p*-nitrophenyl phosphate (Sigma-Aldrich), and the intensity was read at an absorbance of 405 nm. For IgA measurement, goat anti-mouse IgA (Southern Biotech) coupled to horseradish peroxidase (HRP) was added as the secondary antibody at a 1:2000 dilution for 1 h at 37°C, followed by adding TMB (3, 3, 5, 5'- tetramethylbenzidine) peroxidase substrate (Thermo Scientific) for about 15 min. The reactions were stopped by 1M sulfuric acid, and the intensity was read at an absorbance of 450 nm.

**Cytokine measurement by ELISA.** TNF- $\alpha$ , IL-6, and IL-12p70 production were measured using the cytokine kits purchased from Invitrogen and following the instructions from the manufacturer.

**ACE2 inhibition assay.** 96-well plates were coated with 1  $\mu$ g/mL of purified SARS-CoV-2 RBD protein overnight at 4°C. Plates were washed with PBS with 0.05% TWEEN-20, followed by blocking with 1% BSA for 45 min at 37°C. Mouse sera were diluted at 1:100 in 1% BSA in PBS were incubated for 30 min at room temperature. Human recombinant ACE2-Fc-tag (Raybiotech) was then added at 1  $\mu$ g/mL and incubated overnight at 4°C, followed by incubation with 0.2  $\mu$ g/ml anti-ACE2 (R&D) for 1 h at room temperature. Rabbit anti-goat IgG-HRP (Santa Cruz) at 1:8000 dilution was added for 30 min at room temperature. TMB was added for 15 min and the reaction was stopped by sulfuric acid. Absorbance at 450 nm and 570 nm were read and the absorbance at 570 nm was subtracted from the absorbance at 450 nm.

**Quantitative PCR (q-PCR).** Viral-infected cells or tissues were resuspended in Trizol (Invitrogen) for RNA extraction. Complementary (c) DNA was synthesized by using a qScript cDNA synthesis kit (Bio-Rad). The sequences of the primer sets for cytokines, SARS-CoV-2 S gene and PCR reaction conditions were described previously.<sup>19-21</sup> The PCR assay was performed in the CFX96 real-time PCR system (Bio-Rad). Gene expression was calculated using the formula  $2^{-[C_t(\text{target gene}) - C_t(\beta\text{-actin})]}$  as described before.<sup>22</sup>

**B cell ELISPOT assay.** ELISPOT assays were performed as previously described<sup>23</sup> with some modifications. Briefly, splenocytes or lung leukocytes were stimulated with 1  $\mu\text{g}/\text{ml}$  R848 and 10  $\text{ng}/\text{ml}$  recombinant human IL-2 (Mabtech In, OH). Millipore ELISPOT plates (Millipore Ltd, Darmstadt, Germany) were coated with 100  $\mu\text{l}$  SARS-CoV-2 RBD (RayBiotech, USA, 10  $\text{mg}/\text{ml}$ ) or rSARS-CoV-2 spike protein (R&D Systems). To detect total IgG or IgA expressing B cells, the wells were coated with 100  $\mu\text{l}$  of anti-mouse IgG or IgA capture Ab (Mabtech In). Stimulated cells were harvested, and added in duplicates to assess total IgG, IgA ASCs, or SARS-CoV-2 specific B cells. The plates were incubated overnight at 37°C, followed by incubation with biotin-conjugated anti-mouse IgG (Mabtech In) for 2 h at room temperature, then 100  $\mu\text{L}/\text{well}$  streptavidin-ALP was added for 1 h. Plates were developed with BCIP/NBT-Plus substrate until distinct spots emerge, washed with tap water, and scanned using an ImmunoSpot 6.0 analyzer and analyzed by ImmunoSpot software (Cellular Technology Ltd).

**IFN- $\gamma$  ELISPOT.** Millipore ELISPOT plates (Millipore Ltd) were coated with anti-IFN- $\gamma$  capture Ab (Cellular Technology Ltd) at 4°C overnight. Splenocytes or lung leukocytes were stimulated in duplicates with SARS-CoV-2 S peptide pools (2  $\mu\text{g}/\text{ml}$ , Miltenyi Biotec) for 24 h at 37°C. Cells were stimulated with anti-CD3 (1  $\mu\text{g}/\text{ml}$ , e-Biosciences) or medium alone were used as controls. This was followed by incubation with biotin-conjugated anti-IFN- $\gamma$  (Cellular Technology Ltd) for 2 h at room temperature, and then alkaline phosphatase-conjugated streptavidin for 30 min. The plates were washed and scanned using an ImmunoSpot 6.0 analyzer and analyzed by ImmunoSpot software to determine the spot-forming cells (SFC) per 10<sup>6</sup> splenocytes.

**Intracellular cytokine staining (ICS).** Splenocytes or lung leukocytes were incubated with SARS-CoV-2 S peptide pools (1  $\mu\text{g}/\text{ml}$ , Miltenyi Biotec) for 24 h. BD GolgiPlug (BD Bioscience) was added to block protein transport at the final 6 h of incubation. Cells were stained with antibodies for CD3, CD4, or CD8, fixed in 2% paraformaldehyde, and permeabilized with 0.5% saponin before adding anti-IFN- $\gamma$ , or control rat IgG1 (e-Biosciences). Samples were processed with a C6 Flow Cytometer instrument. Dead cells were excluded based on forward and side light scatter. Data were analyzed with a CFlow Plus Flow Cytometer (BD Biosciences).

**Immunofluorescence staining.** SAEC and RPMI2650 cells were seeded in 8-well chamber slides at a density of  $3 \times 10^4$  cells per well and cultured overnight. Fluorescent vaccine particles were prepared using Cy5 labeled CpG ODN, and then incubated with cells at the

ratio of 10–1 between mPSM to cells for 6 h. After incubation, cells were washed with PBS twice, fixed with 4% paraformaldehyde at room temperature for 15 min, and permeabilized with 0.1% tween-20 for 15 min. After blocking with 1% BSA plus 5% FBS, cells were incubated with anti-EEA1 antibody (1:500, Abcam) at 4°C overnight, followed by staining with AF488 -labeled goat anti-rabbit secondary antibody (1:1000 dilution, ThermoFisher) at room temperature for 2 h. Finally, nuclei were stained with 0.5  $\mu\text{g}/\text{mL}$  DAPI for 15 min.

**mNeonGreen (mNG) SARS-CoV-2 reporter neutralization assay.** The mNG reporter USA-WA1/2020 SARS-CoV-2 neutralization assay was performed using a previously described method with some modifications.<sup>24</sup> Vero CCL-81 cells ( $1.2 \times 10^4$ ) in 50  $\mu\text{l}$  of DMEM containing 2% FBS were seeded in each well of black  $\mu\text{CLEAR}$  flat-bottom 96-well plate (Greiner Bio-one™). The cells were incubated overnight at 37°C with 5% CO<sub>2</sub>. On the next day, each serum in duplicate was 2-fold serially diluted in DMEM with 2% FBS and incubated with mNG SARS-CoV-2 at 37°C for 1 h. The virus-serum mixture was transferred to the Vero CCL-81 cell plate with the final multiplicity of infection (MOI) of 0.5. For each serum, the starting dilution was 1/50 with nine 2-fold dilutions to the final dilution of 1/12800. After incubating the infected cells at 37°C for 16–24 h, 25  $\mu\text{l}$  of Hoechst 33342 Solution (400-fold diluted in Hank's Balanced Salt Solution; Gibco) was added to each well to stain the cell nucleus. The plate was sealed with Breath-Easy sealing membrane (Diversified Biotech), incubated at 37°C for 20 min, and quantified for mNG fluorescence on Cytation™ 7 (BioTek). The raw images (1 picture per well) were acquired using 4  $\times$  objective. Infection rates were determined by dividing the mNG positive cell number by total cell number (indicated by nucleus staining). Relative infection rates were obtained by normalizing the infection rates of serum-treated groups to those of non-serum-treated controls. The curves of the relative infection rates versus the serum dilutions (Log<sub>10</sub> values) were plotted using Prism 8 (GraphPad). A nonlinear regression method was used to determine the dilution fold that neutralized 50% of mNG fluorescence (mNG-NT<sub>50</sub>).

**Plaque assay.** Vero E6 cells were seeded on 6-well plates and incubated at 37°C, 5% CO<sub>2</sub> for 16 h. Lung tissue homogenates in 0.2 ml volumes were used to infect the cells for 1 h. After the incubation, the overlay medium containing MEM with 2% FBS, 1% penicillin–streptomycin, and 1.6% agarose was added to the infected cells. Plates were stained with neutral red (Sigma-Aldrich) and plaques were counted to calculate viral titers expressed as PFU/ml.

**Statistical analysis.** Values for viral load, cytokine production, antibody titers, and T cell response experiments were compared using Prism software (Graph-Pad) statistical analysis and were presented as means  $\pm$  SEM. *P* values of these experiments were calculated with a non-paired Student's *t* test.

**Study approval.** All experiments were performed in compliance with and under the approval of the Animal Care and Use Committee at UTMB.

## RESULTS

mPSM is a potent adjuvant for SARS-CoV-2 RBD subunit vaccine and triggers SARS-CoV-2 -specific antibody production with minimal adverse effects upon parenteral vaccination in mice. The RBD of SARS-CoV-2 S protein is considered to be the major protective antigen, which elicits highly potent neutralization

antibodies.<sup>4</sup> To express and purify the S RBD domain, a DNA fragment encoding amino acid residues 319–541 of SARS-CoV-2 S protein was cloned into the lentivirus vector pCDH-CMV-MCS-EF1 $\alpha$ -RFP which was then applied to transduce 293FT cells. To facilitate the secretion and purification of the protein, the first 19 residues of the S protein and a hexahistidine (6xHis) tag were fused at the N-terminal as a secretion signal and the C-terminal respectively. The recombinant RBD protein (25–30 kDa) was purified from the cell culture supernatant (Fig 1, A and B). The protein antigen was packaged into mPSM to prepare a SARS-CoV-2 RBD subunit vaccine (mPSM-RBD) following our recently described protocol.<sup>17</sup> To assess the effects of mPSM-RBD on DC activation and antigen presentation, bone marrow-derived DCs (BMDCs) isolated from BALB/c mice were treated with PBS (mock), RBD alone or together with either Alum, or mPSM.

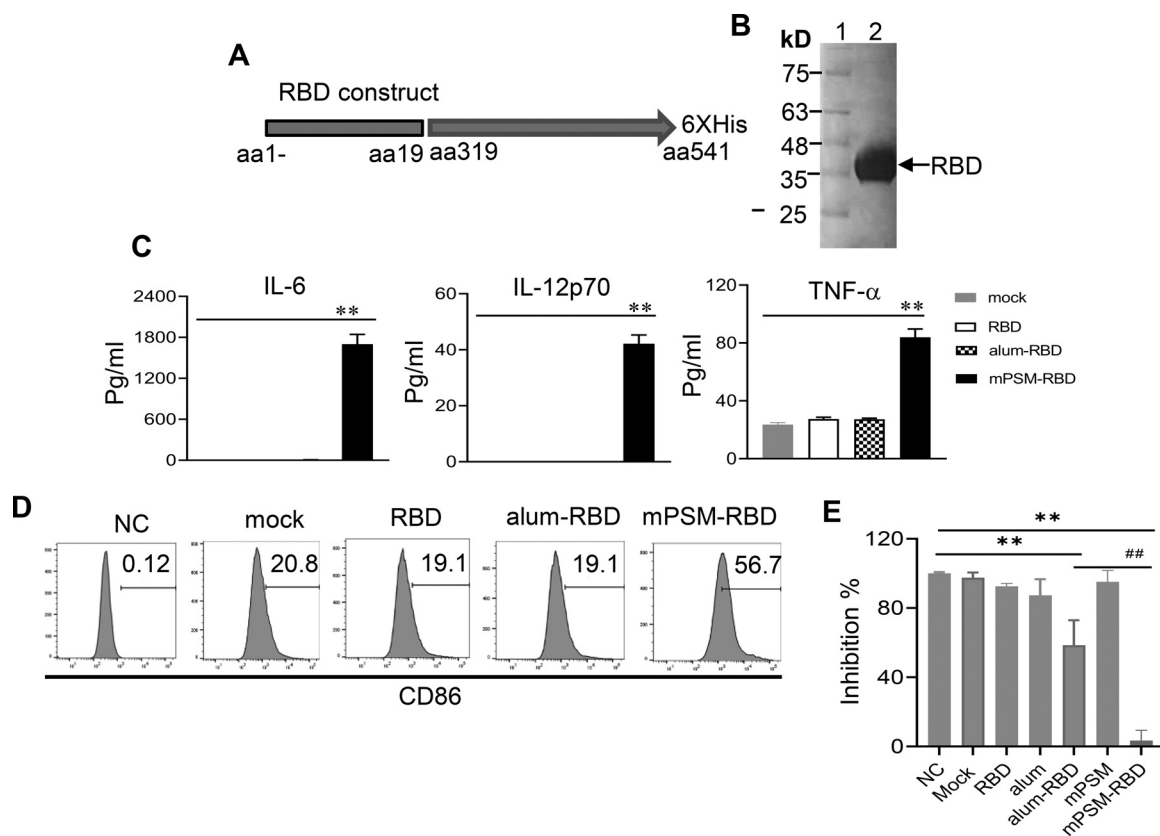


**Fig 1.** mPSM serves a potent adjuvant for SARS-CoV-2 RBD vaccine to generate SARS-CoV-2 specific antibodies in mice following parenteral vaccination. (A) Schematic of SARS-CoV-2 RBD construct. (B) Coomassie blue staining of purified recombinant (r)RBD protein. Lane 1: protein molecular weight marker. C-D. Cytokine production and activation of cell surface CD86 expression in BMDCs treated with mPSM-RBD and controls. (C) Levels of IL-6, IL-12p70 and TNF- $\alpha$  in cell culture supernatant were determined by ELISA 24 h after the treatment. *n* = 3. (D) CD86 expression was measured by flow cytometry analysis. One representative image is shown. (E) ACE2 competition assay. Sera of mice-vaccinated with mPSM-RBD, alum-RBD, RBD, and mock were collected at 1 month postvaccination to measure the inhibitory effects on RBD binding to its receptor ACE2. *n* = 3–4. \*\* *P* < 0.01 compared to mock group. ## *P* < 0.01 compared to alum-RBD group.

The production of pro-inflammatory cytokines, including IL-6, IL-12p70, and TNF- $\alpha$  was markedly increased in mPSM-RBD-treated but not in alum-RBD- or mock-treated DCs. Cell surface co-stimulation molecules, such as CD80 and CD86 expression was also enhanced in the mPSM-RBD-treated, but not in the alum-RBD-treated DCs (Fig 1, C and D, Fig. S1, A), which together suggest a role of mPSM in promoting activation of antigen presenting cells (APC). To assess whether mPSM-RBD vaccination produces SARS-CoV-2-specific antibody responses, sera of mice vaccinated with RBD alone, alum-RBD, or mPSM-RBD were collected one month postvaccination to determine their inhibitory effects on RBD binding to its receptor ACE2. While serum from alum-RBD-vaccinated mice diminished RBD binding to ACE2, that from mPSM-RBD-treated mice nearly abolished binding of ACE2 to RBD protein (Fig 1, E). Routes of parenteral vaccination were also compared. Mice were primed and boosted with mPSM-RBD (5  $\mu$ g) via i.d., i. m., or i.p. inoculation. All 3 routes of inoculation resulted in high titers of RBD-binding IgG2a, IgG2b, and IgG1 subtypes IgG antibodies at one month postvaccination (Fig. S1, B). To further assess the effects of mPSM-RBD dosing in mice, mice were vaccinated i.d. with 1–50  $\mu$ g mPSM-RBD. Interestingly, vaccination with as little as 5  $\mu$ g mPSM-RBD triggered similar levels of IgG2b responses as elicited by 25 and 50  $\mu$ g mPSM-RBD, which remained high more than 180 days postvaccination. However, 25 and 50  $\mu$ g mPSM-RBD triggered much stronger IgG2a and IgG1 responses than the 5  $\mu$ g mPSM-RBD group (Fig. S1, C). Lastly, mPSM-RBD was applied to evaluate potential toxicity, and biomarkers including urea nitrogen (BUN), albumin (ALB), calcium (CA), creatinine (CRE), glucose (GLU), phosphorus (PHOS), and total protein (TP) were assessed. No significant difference between mPSM-RBD and PBS control was observed (Fig. S1, D), which indicates no severe toxicity from mPSM-RBD in mice. Overall, these results suggest that mPSM serves as a potent and safe adjuvant for SARS-CoV-2 RBD subunit vaccine.

Parenteral vaccination with mPSM-RBD subunit vaccine generated strong and durable systemic SARS-CoV-2-specific humoral and type 1 helper T (Th) cell-mediated immune responses, but modest mucosal immune responses in mice. BALB/c and C57BL/6 mice were i.d. inoculated with PBS control, alum-RBD (5  $\mu$ g), or mPSM-RBD (5  $\mu$ g) on day 0 and boosted with the same dose on day 14. Sera were collected at days 7, 14 and 21 to determine antibody titers (Fig 2, A). mPSM-RBD group showed  $10^3$ – $10^7$  titers of RBD binding total IgG or IgG subtype antibodies (IgG2a, IgG2b, and IgG1) on days 7, 14 and 21. In comparison, alum-RBD

vaccination barely induced any RBD IgG2a and IgG2b antibodies, and only low titers of RBD-binding IgG or IgG1 antibodies after day 14 (Fig 2, B). While both alum-RBD and mPSM-RBD produced similar levels of RBD-binding IgG1 antibodies in B6 mice, only the latter induced RBD-specific IgG2b responses (Fig S2, A and B). On day 30, mPSM-RBD-vaccinated BALB/c mice had over 3-fold more SARS-CoV-2 S-specific IgG<sup>+</sup> splenic B cells (Fig 2, C and D) and the splenocytes produced over 8-fold higher IFN- $\gamma$  upon *in vitro* re-stimulation with S peptide pools compared to the alum-RBD group (Fig 2, E and F). mPSM-RBD vaccination also triggered more robust SARS-CoV-2-specific splenic B and T cell responses in B6 mice compared to alum-RBD vaccine (Fig S2, C–F). Cytokines secreted by Th1 cells are known to mediate isotype switching to IgG2a, whereas cytokines secreted by Th2 cells mediate isotype switching to IgG<sub>1</sub>.<sup>25</sup> Thus, the mPSM-RBD vaccine promotes strong systemic humoral and Th1-prone immune responses in mice. Furthermore, there were higher IFN- $\gamma$ -producing CD4<sup>+</sup> and CD8<sup>+</sup> T cell responses, more IgA<sup>+</sup> B cells induced in the lung and stronger IgA antibodies detected in the bronchoalveolar lavage fluids (BAL) of mPSM-RBD-vaccinated mice compared to the mock or alum-RBD group, though the overall magnitude of mucosal immune responses were modest compared to systemic immune responses (Fig 2, G–I, Fig S2, G and H).

To assess the durability of mPSM-RBD-induced immunity, BALB/c mice were immunized i.d. with PBS (mock), mPSM-RBD (5  $\mu$ g), or Alum-RBD (5  $\mu$ g) on days 0 and 14. Longitudinal sera samples were collected over the course of 7 months to determine SARS-CoV-2-specific antibody responses (Fig 3, A). mPSM-RBD vaccination triggered the production of SARS-CoV-2 RBD-binding IgG2a, IgG2b and IgG1 antibodies on day 10, which reached to the peak response around 4 weeks but remained high even at 7 months postvaccination. In contrast, RBD-binding IgG2a and IgG2b antibodies were barely detectable except for lower IgG1 responses in alum-RBD-vaccinated mice (Fig 3, B–D). In addition, mPSM-RBD-vaccinated mice showed more than 100 times higher titers of RBD-binding total IgG 4.5 months postvaccination compared to mice treated with alum-RBD (Fig S3, A and B). Furthermore, high Nab titers against SARS-CoV-2 USA-WA1/2020 strain were detected at 1 month in the majority of mPSM-RBD-vaccinated mice and remained at a similar level 5 months later in all vaccinated mice; in comparison, Nab was barely detectable in any alum-RBD-vaccinated mice throughout the time (Fig 3, E). While both mPSM-RBD and alum-RBD vaccinations induced RBD-specific IgG<sup>+</sup> B cell responses, there were 2.5-fold as many S-specific

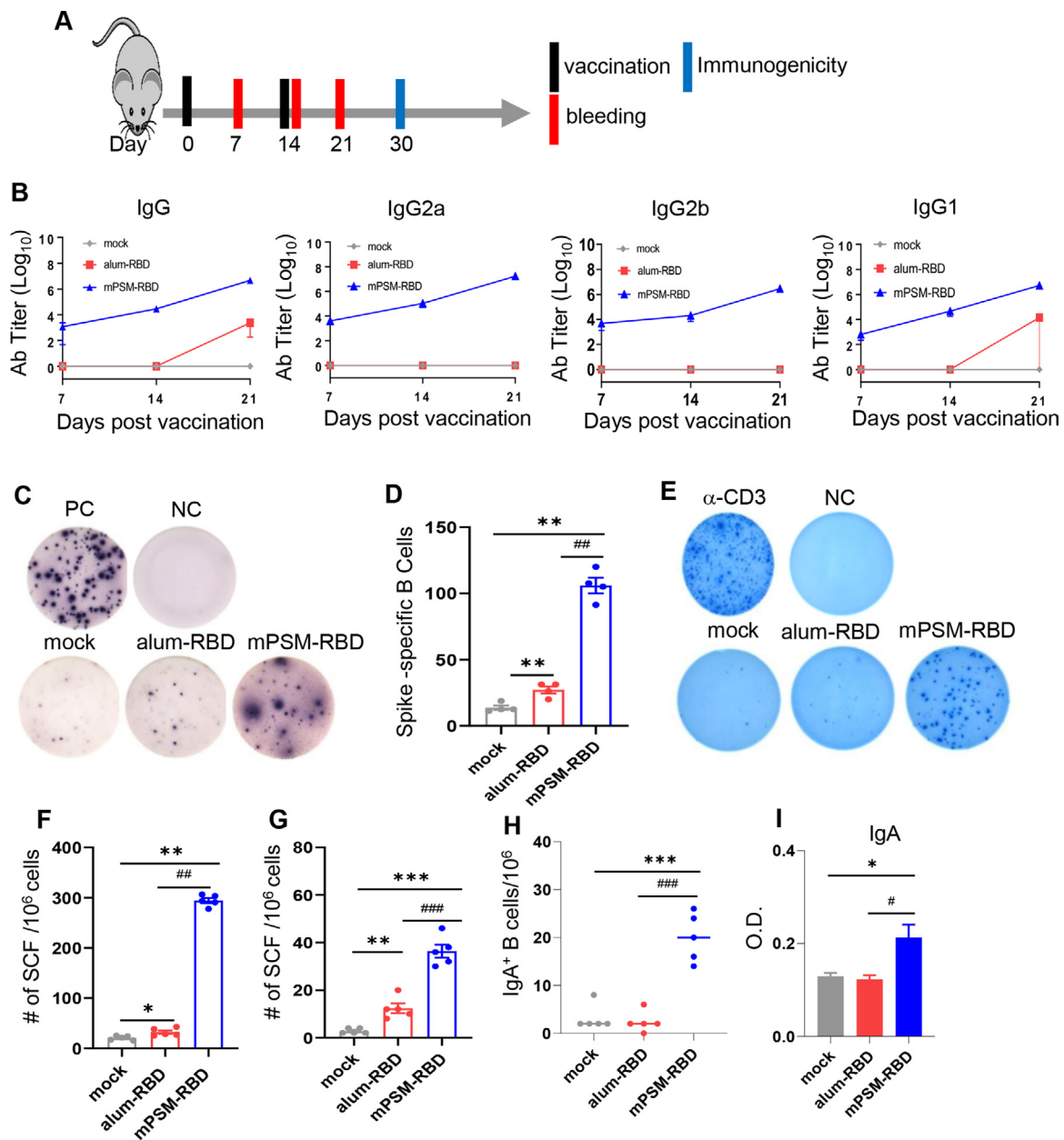


**Fig 2.** mPSM-RBD induced strong systemic but modest mucosal immune responses in BALB/c mice at one month postparenteral vaccination. (A) Study design and vaccination timeline. (B) Endpoint total IgG or IgG subtype titers against SARS-CoV-2 RBD measured in serum collected from the vaccinated mice. *n* = 5. (C and D) SARS-CoV-2 specific memory B cell (MBC) responses by ELISPOT analysis. (C) Images of wells from MBC culture. Splenocytes were stimulated for 7 d with R848 plus rIL-2 and seeded onto ELISPOT plates coated with Ig capture Ab or SARS-CoV-2 RBD. Images of total IgG-antibody secreting cells (ASC), RBD-specific MBCs, and negative control (NC) wells are shown. (D) Frequencies of SARS-CoV-2 RBD-specific ASCs per 10<sup>6</sup> input cells in MBC cultures from the subject. *n* = 4. (E and F) ELISPOT quantification of vaccine-specific T cells. Splenocytes were stimulated with overlapping peptide pools spanning SARS-CoV-2 S protein, α-CD3, or blank (NC) for 20 h. (E) Images of wells from T cell culture. (F) Spot forming cells (SFC) were measured by IFN-γ ELISPOT. Data are shown as # of SFC per 10<sup>6</sup> splenocytes. *n* = 5. (G) ELISPOT assay of SARS-CoV-2-specific lung T cells. Lung leukocytes were stimulated with SARS-CoV-2 S peptides for 20 h. Spot forming cells (SFC) were measured by IFN-γ ELISPOT. *n* = 5. (H) Lung leukocytes were stimulated *in vitro* for 7 days with R848 plus rIL-2 and seeded onto ELISPOT plates coated with SARS-CoV-2 RBD. Frequencies of SARS-CoV-2 RBD specific IgA secreting lung B cells per 10<sup>6</sup> input cells in MBC cultures. *n* = 5. I. IgA titers in BAL. \*\*\* *P* < 0.001, \*\* *P* < 0.01, or \* *P* < 0.05 compared to mock group. ### *P* < 0.001, ## *P* < 0.01, or # *P* < 0.05 compared to alum- RBD group.

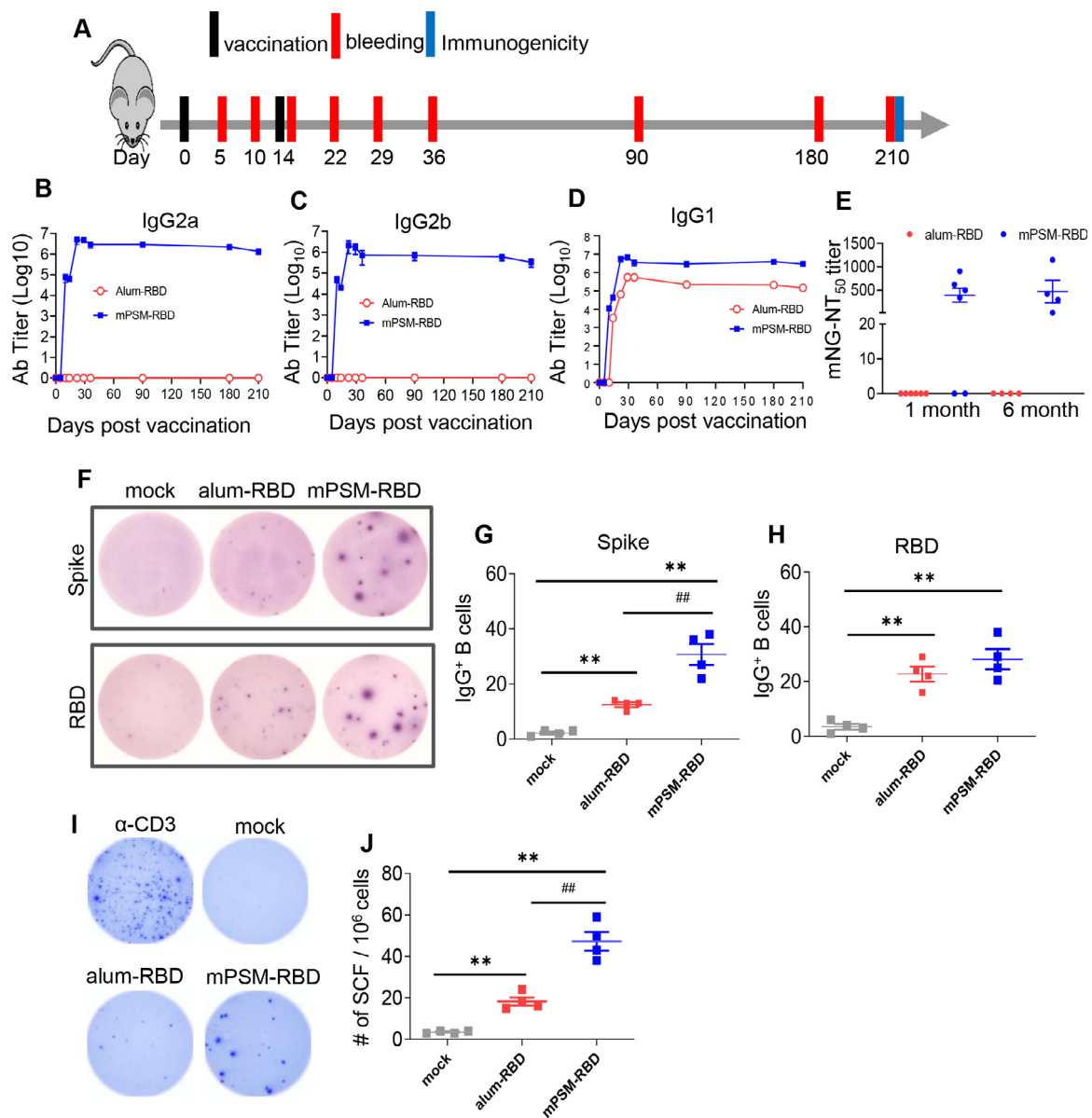


**Fig 3.** mPSM-RBD induced durable Type 1 prone protective immunity following parenteral vaccination. BALB/c mice were prime-boost immunized with mock (PBS), alum-RBD, or mPSM-RBD via i.d. route. (A) Study design. (B–D) Endpoint IgG subtype titers against SARS-CoV-2 RBD measured in serum.  $n = 4$ . (E) Serum neutralizing activity against mNG USA-WA1/2020 was measured by plaque reduction neutralization test (PRNT). mNG-NT<sub>50</sub> titers are shown,  $n = 4$  or 6. (F–H) SARS-CoV-2 specific memory B cell (MBC) responses by ELISPOT analysis at 7 months postvaccination. (F) Images of wells from MBC culture. Frequencies of spike (G) or RBD (H) specific ASCs per  $10^6$  input cells in MBC cultures from the subject. (I and J) ELISPOT quantification of vaccine-specific splenic T cells at 7 months postvaccination. Splenocytes were stimulated with SARS-CoV-2 S peptides,  $\alpha$ -CD3, or blank for 20 h. (I) Images of wells from T cell culture. (J) Spot forming cells (SFC) were measured by IFN- $\gamma$  ELISpot. Data are shown as # of SFC per  $10^6$  splenocytes.  $n = 4$ . \*\*  $P < 0.01$  compared to the mock group. ##  $P < 0.01$  compared to alum-RBD group.

IgG<sup>+</sup> splenic B cells and 1.5-fold as many SARS-CoV-2-specific splenic Th1 type cells in the mPSM-RBD group compared to the alum-RBD group 7 months postvaccination (Fig 3, F–J). Both mPSM-RBD and alum-RBD-vaccinated mice had modest levels of SARS-CoV-2 S-specific splenic IgA<sup>+</sup> B cells, which

were not detectable in the lung (Fig S3, C–E). There were SARS-CoV-2-specific Th1 responses induced in the lung of mPSM-RBD group but not in mock or alum-RBD groups (Fig. S3, F). Taken together, parenteral vaccination with mPSM-RBD induced stronger and more durable systematic SARS-CoV-2-specific

IgG<sup>+</sup> B cells, higher Nab titers and Th1-prone immune responses than alum-RBD in mice. However, compared to systemic immune responses in mPSM-RBD mice, mucosal immune responses were modest. mPSM-RBD provides more durable and potent protection against SARS-CoV-2 strain CMA4 and Beta variant infection following single or 2-dose parenteral vaccination in mice. To assess the efficacy of mPSM-RBD in host protection against SARS-CoV-2 infection, BALB/c mice were vaccinated with alum-RBD (5  $\mu$ g), mPSM-RBD (5  $\mu$ g), or mock i.p. on day 0 and boosted with the same dose on day 21. At 1 month postvaccination, mice were i.n. challenged with  $2 \times 10^4$  PFU mouse-adapted SARS-CoV-2 strain CMA4.<sup>18</sup> Viral replication and virus-induced inflammatory responses in the lung are associated with SARS-CoV-2 susceptibility.<sup>6,26</sup> Thus, viral loads and pro-inflammatory cytokines and chemokine mRNA levels in the lung were used to evaluate the protective efficacy. Mice were euthanized 2 days after infection (Fig S4, A). There were lower viral loads and attenuated levels of inflammatory cytokines, including CCL2, CCL7 and CXCL10 in the lung of mPSM-RBD group compared to the mock group. Alum-RBD- vaccinated mice also showed similar reductions on viral loads and inflammation in the lung (Fig S4, B-E). In another study, mice were i.n. challenged with  $2 \times 10^4$  PFU of the mouse-adapted SARS-CoV-2 strain CMA4 at 4.5 months postvaccination. While mice in both mock and alum-RBD groups exhibited  $10^2$ – $10^3$  PFU/ml viral loads in the lung tissues; no detectable viral titers were measured in the mPSM-RBD group at day 4 postinfection (Fig 4, A and B). The mPSM-RBD-vaccinated mice had significantly reduced levels of lung inflammation compared to the mock and the alum-RBD group (Fig 4, C–H). Furthermore, to assess protective efficacy from a single dose vaccination, 6–8-week-old K18 hACE2 mice were treated i.p. with PBS (mock), alum-RBD (25  $\mu$ g), or mPSM-RBD (25  $\mu$ g). Mice were challenged i.n. with  $4 \times 10^3$  PFU of SARS-CoV-2 Beta variant 1 month postvaccination. While both alum-RBD and mPSM-RBD groups showed reduced viral loads in the lung compared to the mock group, mice in the mPSM-RBD group had more than 1-fold lower viral load in the lungs than those in the alum-RBD group (Fig 4, I and J). In summary, these data showed that the mPSM-RBD vaccine triggered more durable and stronger protection against SARS-CoV-2 and Beta variant infection than the alum-RBD vaccine following single or 2 doses of parenteral vaccination. mPSM promotes nasal and airway epithelial cells uptake of SARS-CoV-2 RBD antigen; Intranasal boost with mPSM-RBD triggers potent SARS-CoV-2 -specific mucosal and systemic immune responses which protect host against SARS-

CoV-2 Delta variant challenge. The magnitude of virus-specific T cells in the lung is known to be associated with better prophylaxis of COVID-19 patients.<sup>27</sup> Mucosal vaccination is likely to be more effective in control of virus spread as it can enhance lung resident memory T cells compared to parenteral injection.<sup>14</sup> To determine whether mPSM could also serve as an efficient carrier for mucosal delivery of SARS-CoV-2 antigen, we assessed RBD antigen uptake by the upper respiratory epithelial cells. Cy5-labeled mPSM-RBD was applied to treat human small airway epithelial cells (SAEC) and human nasal cell line RPMI2650, and intracellular particle trafficking was monitored. Microscopic analysis revealed that mPSM-RBD bound to both SAECs and RPMI2650 cells, with a higher binding affinity to SAECs based on the average number of particles in each cell type (Fig 5, A). mPSM-RBD colocalized with early endosome (EEA1<sup>+</sup>, green) as soon as 0.5 h after incubation. After 2 h and 6 h incubation, mPSM-RBD vaccine was gradually released from the particles and reached the surrounding area inside the cells. These results suggest that mPSM can effectively deliver RBD antigen and promote its uptake by upper respiratory epithelial cells. Next, we assessed SARS-CoV-2- specific immune responses in BALB/c mice following primed i.p. with PBS (mock), RBD alone, m-PSM-RBD or alum-RBD (5  $\mu$ g) on day 0 and boosted i.n. with the same dose on day 21 (Fig 5, B). Blood, BAL, lung and spleen tissues were collected on day 35. In the lung, there were stronger SARS-CoV-2-specific Th1 responses in mPSM-RBD group than the alum-RBD group, and both CD4<sup>+</sup> and CD8<sup>+</sup> T cells produced more IFN $\gamma$  than the alum-RBD group (Fig 5, C–E). The mPSM-RBD group produced at least 2-fold as many RBD-specific IgA<sup>+</sup> B cells in the lung and nearly 44-fold higher IgA antibodies in the BAL compared to those in the alum-RBD group (Fig 5, F–H). In the spleen, the mPSM-RBD group also showed elevated levels of IFN $\gamma$ - production than the alum-RBD group. Among splenic T cells, CD8<sup>+</sup> T cells, but not CD4<sup>+</sup>T cells, produced significantly more IFN $\gamma$  in the mPSM-RBD group than the alum-RBD group (Fig S5, A–C). There were more SARS-CoV-2 specific IgA<sup>+</sup> splenic B cells induced in the mPSM-RBD-vaccinated mice (Fig S5, D). Furthermore, higher titers of RBD-binding total IgG, IgA, IgG1 and IgG2a subtype antibodies were detected in sera of mPSM-RBD- vaccinated mice compared to that of alum-RBD- vaccinated mice (Fig S5, E–H). Lastly, to determine the effects of i.p/i.n. prime and boost vaccination with mPSM-RBD in host protection against SARS-CoV-2 variant infection, K18 hACE2 mice were vaccinated i.p. with PBS (mock), RBD (5  $\mu$ g), m-PSM-RBD (5  $\mu$ g), alum-RBD (5  $\mu$ g) on day 0 and boosted i.n. with the same dose on day 21.

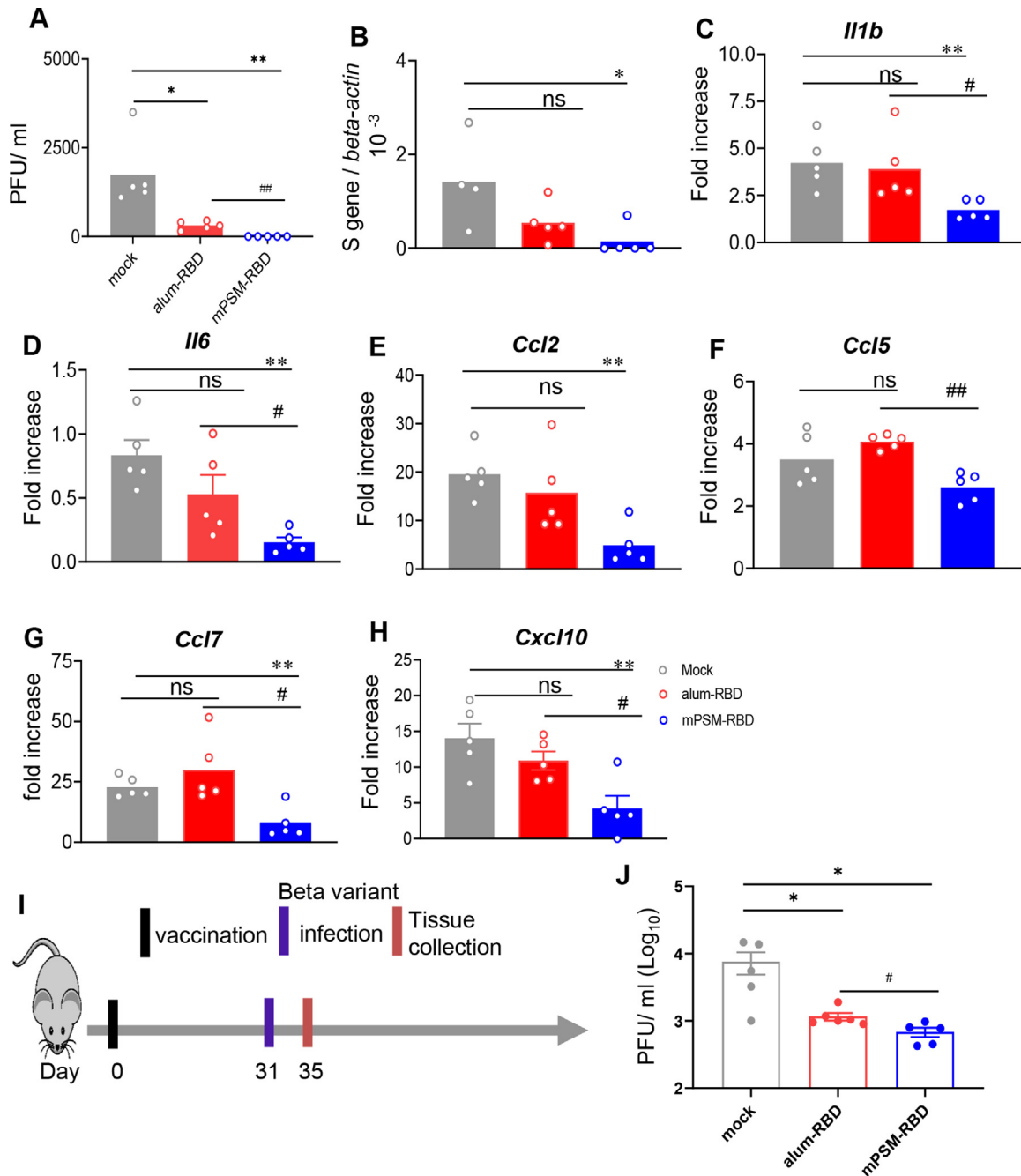


**Fig 4.** The protective efficacy of mPSM-RBD vaccine against SARS-CoV-2 and the Beta variant infection following single or 2 dose parenteral vaccination. (A–H) BALB/c mice ( $n=5$ ) were prime-boost immunized with mock (PBS), alum-RBD, or mPSM-RBD. At 4.5 months postvaccination, mice were i.n. challenged with  $2 \times 10^4$  PFU mouse-adapted SARS-CoV-2 CMA4. (A and B) SARS-CoV-2 viral loads in lung tissues were measured by plaque (A) and Q-PCR (B) assays at day 4 postinfection (pi). (C–H) Cytokine and chemokine levels in lung tissues at day 4 pi. Data are presented as the fold increase compared to naïve mice (means  $\pm$  SEM). (I and J) K18 ACE2 mice ( $n=5$ ) were immunized once i.p. with mock (PBS), alum-RBD, or mPSM-RBD ( $25 \mu\text{g}$ ). At 1 month, mice were i.n. challenged with 4000 PFU SARS-CoV-2 Beta variant. (I) Study design. (J) Viral titers in lung tissues were measured at day 4 pi. \*\*  $P < 0.01$  or \*  $P < 0.05$  compared to mock group. #  $P < 0.05$  or ##  $P < 0.01$  compared to alum-RBD group.

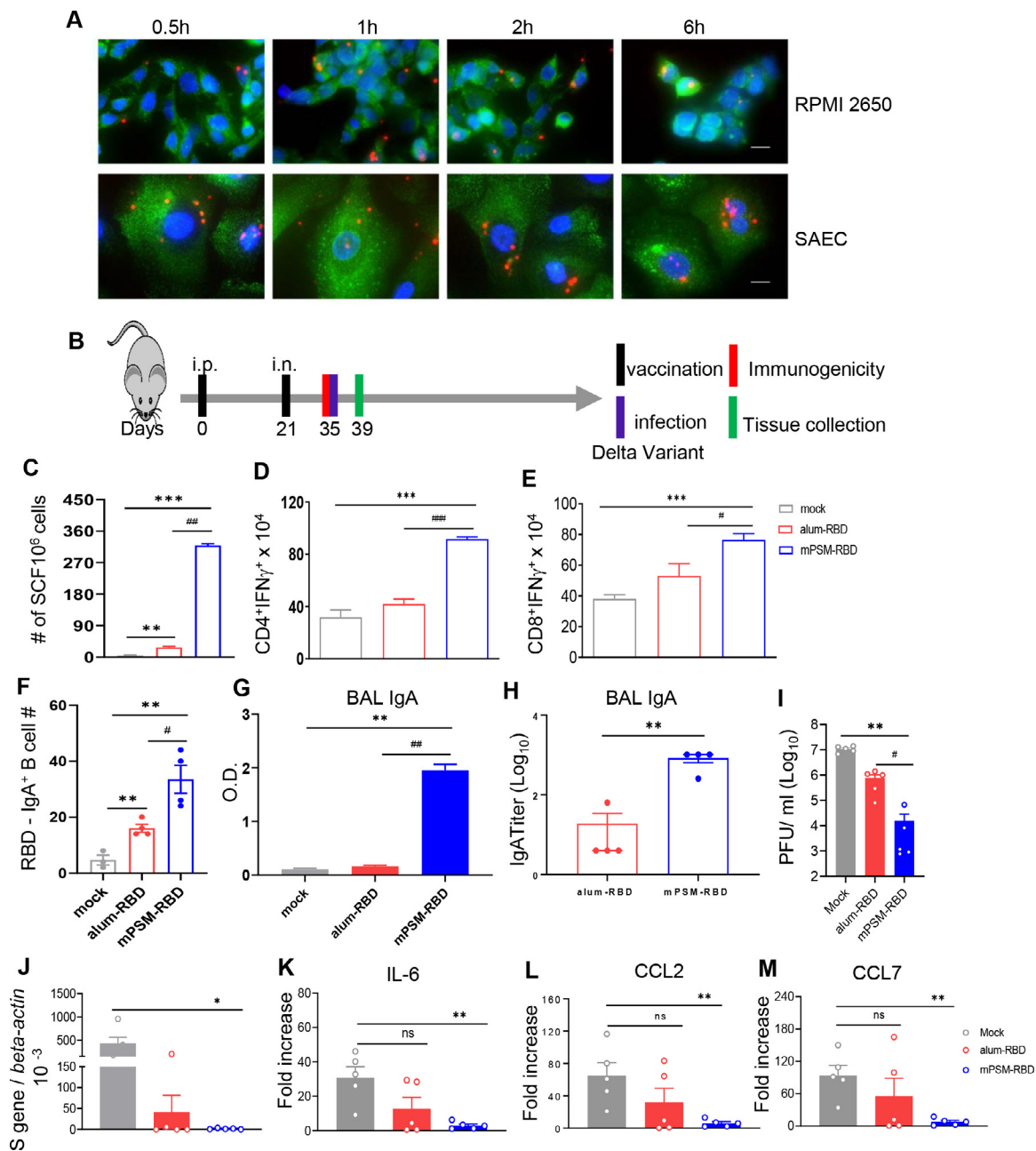


**Fig 5.** Parenteral and mucosal prime-boost vaccination promotes strong mucosal immune responses and provides host protection against SARS-CoV-2 Delta variant infection. (A) Fluorescence microscopic analysis on time-dependent uptake of vaccine particles in human small airway epithelial cells (SAEC) and human nasal cell line RPMI2650. Cells were incubated with Cy5-labeled vaccine particles (red) for indicated times followed by staining with anti-EEA1 (green) and DAPI for nuclei (blue). Bar indicates 10  $\mu$ m. (B) Study design for vaccination and viral challenge. (C–J) Immunogenicity studies at 1 month postvaccination in BALB/c mice. (C) ELISPOT assay of SARS-CoV-2 -specific lung T cells. Lung leukocytes were stimulated with SARS-CoV-2 S peptides for 20 h. Spot forming cells (SFC) were measured by IFN- $\gamma$  ELISPOT. n = 3–4. (D and E) Lung leukocytes were cultured *ex vivo* with S peptide pools for 5 h, and stained for IFN- $\gamma$ , CD3, and CD4 or CD8. Total number of IFN- $\gamma$ <sup>+</sup> CD4<sup>+</sup> and CD8<sup>+</sup> T cell subsets is shown. (F) Lung leukocytes were stimulated *in vitro* for 7 days with R848 plus rIL-2 and seeded onto ELISPOT plates coated with SARS-CoV-2 RBD. Frequencies of SARS-CoV-2 RBD specific IgA secreting lung B cells per 10<sup>6</sup> input cells in MBC cultures. n = 3–4. (G and H) IgA titers in BAL. (G) O.D. values by ELISA. (H) Endpoint IgA titers against SARS-CoV-2 RBD. (I–M) At day 35 postprime/boost vaccination, all mice were i.n. challenged with 1  $\times$  10<sup>4</sup> PFU SARS-CoV-2 Delta variant. Four days after viral challenge, lung tissues were collected. SARS-CoV-2 viral titers in lung tissues were

Mice were then i.n. challenged with  $1 \times 10^4$  PFU of SARS-CoV-2 Delta variant at day 35. On day 4 postinfection, plaque and Q-PCR assays showed that mPSM-RBD group had about 685-fold and 50-fold decrease in lung viral loads compared to the mock and alum-RBD groups, respectively (Fig 5, I, J). In addition, the mPSM-RBD-vaccinated mice also had significantly diminished levels of lung inflammatory cytokines compared to those in the mock group; in comparison, no difference was detected between the alum-RBD and mock groups (Fig 5, K–M). These studies demonstrated that i.n. boost following parenteral prime with mPSM-RBD vaccine triggers strong mucosal and systemic B cell and Th1-type immune responses and IgA production and protects the host against SARS-CoV-2 Delta variant challenge. Sera from alum-RBD and mPSM-RBD vaccinated groups showed neutralization titers less than 20 against Omicron SARS-CoV-2 variant. Low levels of neutralization titers were also noted in both groups following parenteral prime and boost vaccinations (Fig S6, A and B).

## DISCUSSION

B cell and antibody responses are critical for virus neutralization and disease control but are often of limited duration and breadth during SARS-CoV or SARS-CoV-2 infection.<sup>28</sup> Indeed, some convalescent COVID-19 patients showed variable and sometimes low NAb titers, suggesting other immune factors contribute to the recovery from virus-induced diseases.<sup>29</sup> T cells are also known to play an important role in the clearance of SARS-CoV infection and host protection.<sup>30–32</sup> Chen et al reported that SARS-CoV-2 infection caused a decrease in CD4<sup>+</sup> and CD8<sup>+</sup> T cell counts, and suppressed IFN- $\gamma$  production by CD4<sup>+</sup> T cells, which were associated with the disease severity of COVID-19.<sup>33</sup> Thus, balanced humoral and Th-1 directed cellular immune responses are important host protection against SARS-CoV-2 infection.<sup>34</sup> The S protein, including RBD, can elicit highly potent and persistent NAb and contain many T cell epitopes.<sup>3</sup> Therefore, adjuvanted S or RBD protein subunit vaccines represent some of the most viable strategies for rapidly eliciting SARS-CoV-2 NAb and CD4<sup>+</sup> T cell responses of various qualities depending on the adjuvant used. Currently, the most commonly used adjuvants in human vaccination, such as alum, are effective at enhancing serum antibody titers, but not Th

responses.<sup>35,36</sup> A single dose vaccination with S protein formulated with alum alone induced a more Th2 prone response in mice.<sup>37</sup> Modified alum-based subunit vaccines including adding T helper epitope with RBD antigen or combining a TLR7/8 agonist with alum have been shown to effectively trigger strong humoral immunity supplemented with cellular immunity in mice and enhance NAb titers in various animal models.<sup>38,39</sup> Here, we found that mPSM serves as a better adjuvant than alum for SARS-CoV-2 RBD subunit vaccines to elicit stronger and more durable Nabs, plus memory B cell and Th1 skewed immune responses in mice following parenteral and mucosal vaccination.

The PSMs contain 40–80 nm pores that can be loaded with nanoparticles, which were preferentially internalized by DCs over other types of phagocytic cells inside the body. Once inside the cells, PSM slowly degrades into non-toxic orthosilicic acid, a process that can last for as long as 2 weeks and the cargo inside the nanopores is gradually released.<sup>40,41</sup> Thus, PSM acts as a reservoir for sustained release of antigen and other stimulatory factors, which offers the benefit of long-term stimulation of the APCs to trigger long-lasting immunity. Furthermore, PSM was previously reported to stimulate TRIF/MAVS-mediated pathways leading to activation of type I IFN responses.<sup>16</sup> mPSMs, which includes PSM CpG and cGAMP elicits stronger innate cytokine response and more potent Th-1 biased immune responses, possibly due to the synergistic immune responses via multiple intracellular signaling pathways.<sup>17</sup>

Intranasal immunization can lead to the induction of antigen-specific immunity in both the mucosal and systemic immune compartments.<sup>14</sup> Delivery of antigens to the sites of infection and induction of mucosal immune responses in the respiratory tract, including IgA and resident memory B and T cells provides 2 additional layers of protection compared to systemic vaccination.<sup>42</sup> Induction of mucosal IgA antibodies has been shown to help control several other respiratory viruses, such as SARS-CoV and RSV.<sup>43–45</sup> Compared to IgG, IgA has been shown to more effectively control SARS-CoV-2 infection in the upper respiratory tract and nasal passages.<sup>46</sup> Thus, mucosal vaccination appears to be more effective in control of SARS-CoV-2 infection and disease.<sup>47,48</sup> Current delivery of the EUA SARS-CoV-2 vaccines is limited to parenteral injection, such as intramuscular route. In fact, less than 10% of the total 100 COVID-19 vaccines currently undergoing

measured by plaque (I) and Q-PCR (J) assays. (K–M) Measurement of cytokine and chemokine levels in lung tissues by Q-PCR assays at day 4 postinfection. Data are presented as the fold increase compared to naïve mice (means  $\pm$  SEM).  $n = 5$ . \*\*\*  $P < 0.001$ , \*\*  $P < 0.01$ , or \*  $P < 0.05$  compared to mock group. ###  $P < 0.001$ , ##  $P < 0.01$ , or #  $P < 0.05$  compared to alum-RBD group.

clinical trials utilizes the intranasal route.<sup>42</sup> However, soluble antigens delivered to the nasal passages do not breach the epithelium but are transported across the epithelial barrier by specialized microfold cells to present to DCs located underneath the epithelium.<sup>15</sup> Embedded in the submucosa is the nasal-associated lymphoid tissue (NALT), which is the first site for inhaled antigen recognition in the upper respiratory tract and includes B cells, T cells, and APCs. Formulation, size, and antigen type are important factors in mucosal vaccine development because they are critical for induction of mucosal immunity. Nanoparticles with size ranging from 20 to 200 nm<sup>49</sup> can serve as carriers for drug delivery to penetrate the mucosal surface and increase retention in the lung.<sup>50</sup> mPSMs were previously reported to get trapped in endosomes for an extended amount of time, a process that benefits both DC activation and antigen processing.<sup>16,17</sup> Although mPSM-RBD induces modest mucosal immunity following parenteral vaccination, mPSM promotes the uptake of SARS-CoV-2 RBD antigens by nasal and airway epithelial cells. Moreover, due to relatively rapid turnover rates of mucosal antibody and lung-resident memory T cells, we applied a 'prime and pull' vaccination strategy.<sup>51</sup> This begins with conventional parenteral vaccination to elicit systemic long-lived IgG response and broader repertoire memory B and T cells (prime), followed by an intranasal boost to recruit memory B and T cells to local lung resident memory cells and IgA production (pull) to mediate protective immunity. We found that the parenteral and mucosal prime-boost vaccination elicited robust SARS-CoV-2-specific systemic and mucosal IgA and Th1-skewed immune responses, which provide host protection against more virulent SARS-CoV-2 Delta variant infection.

Since the pandemic started, several major new variants have been identified as associated with increased viral transmission and disease severity in COVID-19 patients in the United Kingdom, South Africa, Brazil, United States, and more recently in India.<sup>10,11</sup> Among them, the Beta variant, which was first identified in South Africa, has 3 mutations in the SARS-CoV-2 RBD protein, namely K417N, E484K and N501Y. The Delta variant carries 7 mutations in S protein (T19R, G142D, del157/158, L452R, T478K, D614G, P681R).<sup>52</sup> Both Beta and Delta variants are of particular concern for their potential resistance to antibodies elicited by prior SARS-CoV-2 infection and/or vaccination.<sup>53,54</sup> Furthermore, there is a potential concern of "vaccine-induced disease enhancement", which was reported for certain SARS-CoV vaccine candidates<sup>12</sup> and inactivated RSV vaccines.<sup>55</sup> The potential risk of ADE mediated by Fc-receptor could

be increased due to waning immunity after vaccination and possibly mutations in the SARS-CoV-2 S protein.<sup>56</sup> Due to the above concerns, the optimal COVID-19 vaccines will need to exhibit long-lasting immunity, be effective for various populations globally, and provide cross-reactive protection against emerging variants. Here, our results showed that the mPSM-RBD vaccine induced potent and durable Th-1 prone immune responses and protected mice from SARS-CoV-2, Beta and Delta variants infection. Furthermore, the mPSM-RBD vaccine did not cause toxicity in mice.

In this study, we initially applied a 2-week interval for prime and boost vaccinations with mPSM-RBD (Figs 2 and 3). Longer prime-boost intervals have been associated with improved vaccine immunogenicity and increased protective efficacy against SARS-CoV-2 and variants in humans.<sup>57,58</sup> Thus, we also tested a 3-week interval for parenteral and intranasal prime and boost vaccinations with mPSM-RBD, which elicited strong protective mucosal and systemic immune responses (Fig 5). The 3-week interval used for parenteral prime and boost vaccinations also resulted in similar levels of protective systemic immunity as the 2-week interval strategy (Figs 2 and 4). Although mPSM-RBD vaccination protected mice from Beta and Delta variants infection, we noted that the vaccination triggered modest sera neutralizing activities against the Omicron variant. This is not completely unexpected. Compared to previously reported variants, the Omicron variant has more spike mutations, many of which are reported to evade antibody neutralization.<sup>59,60</sup> Our RBD antigen was cloned based on the sequence of the SARS-CoV-2 prototype strain. In future investigations, we will further optimize the immunogenicity of the candidate vaccines by testing alternative vaccine strategy, such as longer than 3-week prime/boost intervals which has been reported to enhance cross-reactive immune responses against SARS-CoV-2 variants in humans.<sup>57,58</sup> In addition, mutant-specific antigens may be included to generate more potent vaccines with the platform. Furthermore, the mouse adaptive strain CMA4 did not trigger significant weight loss nor mortality in BALB/c mice.<sup>18,61</sup> Future optimization studies will also include evaluation of survival rates and/or weight loss in the K18-hACE2 mouse model as well as other feasible animal models, such as hamsters.<sup>62</sup>

In conclusion, we have demonstrated that mPSM is a potent adjuvant for SARS-CoV-2 subunit vaccine and promotes intranasal delivery that triggers robust systemic and mucosal immunity. The mPSM-based platform has been previously used for cancer vaccines to efficiently stimulate protective Th1 immunity.<sup>16,17</sup> It has the potential to replace alum to effectively combat

SARS-CoV-2 and other emerging RNA viruses or infectious pathogens that rely on Th1-mediated immunity.

#### ACKNOWLEDGMENTS

Conflicts of Interest: The authors declare that there are no competing interests. The authors have read the journal's policy on disclosure of potential conflicts of interest and agreed with the journal's authorship statement.

This work was supported in part by NIH grants R01AI127744 (T.W.), R01AI116812 (to X.B.), R21AG069226 (X.B.), U54CA210181 (H.S.), a Fast Grant from Emergent Ventures at the Mercatus Center (T.W.), and a Pilot Grant from the Institute for Human Infections & Immunity (IHII) at UTMB (X.B.).

Author contributions are as follows: A.A., Q.S., B.W., J.Z., J.M., S.R.O., and W.W. performed the experiments. X.B., P.Y.S., H.S., and T.W., designed the experiment. X.X., P.Y.S., and P.V.A. provided critical reagents, A.A., Q.S., J.Z., J.M., and T.W. analyzed the data. T.W. wrote the initial draft of the manuscript and other coauthors provided editorial comments.

We thank Gang Li for technical assistance on the cloning of RBD protein and Dr. Linsey Yeager for assisting in manuscript preparation.

#### SUPPLEMENTARY MATERIALS

Supplementary material associated with this article can be found in the online version at [doi:10.1016/j.trsl.2022.06.004](https://doi.org/10.1016/j.trsl.2022.06.004).

#### REFERENCES

1. Wu A, Peng Y, Huang B, et al. Genome composition and divergence of the novel coronavirus (2019-nCoV) originating in China. *Cell Host Microbe* 2020;27:325–8.
2. Yang Y, Du L. SARS-CoV-2 spike protein: a key target for eliciting persistent neutralizing antibodies. *Signal Transduct Target Ther* 2021;6:95.
3. Li CK, Wu H, Yan H, et al. T cell responses to whole SARS coronavirus in humans. *J Immunol* 2008;181:5490–500.
4. Dai L, Gao GF. Viral targets for vaccines against COVID-19. *Nat Rev Immunol* 2021;21:73–82.
5. Gao Q, Bao L, Mao H, et al. Development of an inactivated vaccine candidate for SARS-CoV-2. *Science* 2020;369:77–81.
6. Hassan AO, Kafai NM, Dmitriev IP, et al. A single-dose intranasal ChAd vaccine protects upper and lower respiratory tracts against SARS-CoV-2. *Cell* 2020;183:169–84, e13.
7. Smith TRF, Patel A, Ramos S, et al. Immunogenicity of a DNA vaccine candidate for COVID-19. *Nat Commun* 2020;11:2601.
8. Walsh EE, Frenck RW Jr., Falsey AR, et al. Safety and immunogenicity of two RNA-based COVID-19 vaccine candidates. *N Engl J Med* 2020;383:2439–50.
9. Wang Y, Yang C, Song Y, et al. Scalable live-attenuated SARS-CoV-2 vaccine candidate demonstrates preclinical safety and efficacy. *Proc Natl Acad Sci U S A* 2021;118.
10. Parums V. Editorial: Revised World Health Organization (WHO) terminology for variants of concern and variants of interest of SARS-CoV-2. *Med Sci Monit* 2021;27:e933622.
11. Plante JA, Mitchell BM, Plante KS, et al. The variant gambit: COVID-19's next move. *Cell Host Microbe* 2021;29:508–15.
12. Liu L, Wei Q, Lin Q, et al. Anti-spike IgG causes severe acute lung injury by skewing macrophage responses during acute SARS-CoV infection. *JCI Insight* 2019;4(4):e123158.
13. Mahmoodpoor A, Sanaie S, Samadi P, et al. SARS-CoV-2: unique challenges of the virus and vaccines. *Immunol Invest* 2021;50:802–9.
14. Teijaro JR, Farber DL. COVID-19 vaccines: modes of immune activation and future challenges. *Nat Rev Immunol* 2021;21:195–7.
15. Kiyono H, Fukuyama S. NALT- versus Peyer's-patch-mediated mucosal immunity. *Nat Rev Immunol* 2004;4:699–710.
16. Xia X, Mai J, Xu R, et al. Porous silicon microparticle potentiates anti-tumor immunity by enhancing cross-presentation and inducing type I interferon response. *Cell Rep* 2015;11:957–66.
17. Mai J, Li Z, Xia X, et al. Synergistic activation of antitumor immunity by a particulate therapeutic vaccine. *Adv Sci (Weinh)* 2021;8:2100166.
18. Muruato A, Vu MN, Johnson BA, et al. Mouse-adapted SARS-CoV-2 protects animals from lethal SARS-CoV challenge. *PLoS Biol* 2021;19:e3001284.
19. Chan JF, Yuan S, Kok KH, et al. A familial cluster of pneumonia associated with the 2019 novel coronavirus indicating person-to-person transmission: a study of a family cluster. *Lancet* 2020;395:514–23.
20. Wang T, Town T, Alexopoulou L, et al. Toll-like receptor 3 mediates West Nile virus entry into the brain causing lethal encephalitis. *Nat Med* 2004;10:1366–73.
21. Xie G, Luo H, Pang L, et al. Dysregulation of toll-like receptor 7 compromises innate and adaptive T cell responses and host resistance to an attenuated West Nile virus infection in old mice. *J Virol* 2016;90:1333–44.
22. Welte T, Aronson J, Gong B, et al. Vgamma4+ T cells regulate host immune response to West Nile virus infection. *FEMS Immunol Med Microbiol* 2011;63:183–92.
23. Adam A, Woda M, Kounlavouth S, et al. Multiplexed FluoroSpot for the analysis of dengue virus- and Zika virus-specific and cross-reactive memory B cells. *J Immunol* 2018;201:3804–14.
24. Muruato AE, Fontes-Garfias CR, Ren P, et al. A high-throughput neutralizing antibody assay for COVID-19 diagnosis and vaccine evaluation. *Nat Commun* 2020;11:4059.
25. Rostamian M, Sohrabi S, Kavosifard H, et al. Lower levels of IgG1 in comparison with IgG2a are associated with protective immunity against *Leishmania tropica* infection in BALB/c mice. *J Microbiol Immunol Infect* 2017;50:160–6.
26. Bao L, Deng W, Huang B, et al. The pathogenicity of SARS-CoV-2 in hACE2 transgenic mice. *Nature* 2020;583:830–3.
27. Melenotte C, Silvain A, Goubet AG, et al. Immune responses during COVID-19 infection. *Oncoimmunology* 2020;9:1807836.
28. Lin Q, Zhu L, Ni Z, et al. Duration of serum neutralizing antibodies for SARS-CoV-2: Lessons from SARS-CoV infection. *J Microbiol Immunol Infect* 2020;53:821–2.
29. Whitman JD, Hiatt J, Mowery CT, et al. Evaluation of SARS-CoV-2 serology assays reveals a range of test performance. *Nat Biotechnol* 2020;38:1174–83.
30. Chen J, Lau YF, Lamirande EW, et al. Cellular immune responses to severe acute respiratory syndrome coronavirus (SARS-CoV) infection in senescent BALB/c mice: CD4+ T cells are important in control of SARS-CoV infection. *J Virol* 2010;84:1289–301.

31. Li T, Qiu Z, Zhang L, et al. Significant changes of peripheral T lymphocyte subsets in patients with severe acute respiratory syndrome. *J Infect Dis* 2004;189:648–51.
32. Zhao J, Zhao J, Perlman S. T cell responses are required for protection from clinical disease and for virus clearance in severe acute respiratory syndrome coronavirus-infected mice. *J Virol* 2010;84:9318–25.
33. Chen G, Wu D, Guo W, et al. Clinical and immunological features of severe and moderate coronavirus disease 2019. *J Clin Investig* 2020;130(5):2620–9.
34. Graham BS. Rapid COVID-19 vaccine development. *Science* 2020;368:945–6.
35. Alving CR, Peachman KK, Rao M, et al. Adjuvants for human vaccines. *Curr Opin Immunol* 2012;24:310–5.
36. Bolhassani A, Rafati S. Mini-chaperones: potential immunostimulators in vaccine design. *Hum Vaccin Immunother* 2013;9(1):153–61.
37. Worzner K, Sheward DJ, Schmidt ST, et al. Adjuvanted SARS-CoV-2 spike protein elicits neutralizing antibodies and CD4 T cell responses after a single immunization in mice. *EBioMedicine* 2021;63:103197.
38. Routhu NK, Cheedarla N, Bollimpelli VS, et al. SARS-CoV-2 RBD trimer protein adjuvanted with Alum-3M-052 protects from SARS-CoV-2 infection and immune pathology in the lung. *Nat Commun* 2021;12:3587.
39. Arunachalam PS, Walls AC, Golden N, et al. Adjuvanting a subunit COVID-19 vaccine to induce protective immunity. *Nature* 2021;594:253–8.
40. Xu R, Huang Y, Mai J, et al. Multistage vectored siRNA targeting ataxia-telangiectasia mutated for breast cancer therapy. *Small* 2013;9:1799–808.
41. Shen H, Rodriguez-Aguayo C, Xu R, et al. Enhancing chemotherapy response with sustained EphA2 silencing using multi-stage vector delivery. *Clin Cancer Res* 2013;19:1806–15.
42. Lund FE, Randall TD. Scent of a vaccine. *Science* 2021;373:397–9.
43. Du L, Zhao G, Lin Y, et al. Intranasal vaccination of recombinant adeno-associated virus encoding receptor-binding domain of severe acute respiratory syndrome coronavirus (SARS-CoV) spike protein induces strong mucosal immune responses and provides long-term protection against SARS-CoV infection. *J Immunol* 2008;180:948–56.
44. Kim S, Jang JE, Yu JR, et al. Single mucosal immunization of recombinant adenovirus-based vaccine expressing F1 protein fragment induces protective mucosal immunity against respiratory syncytial virus infection. *Vaccine* 2010;28:3801–8.
45. Yusuf H, Kett V. Current prospects and future challenges for nasal vaccine delivery. *Hum Vaccin Immunother* 2017;13:34–45.
46. Wang Z, Lorenzi JCC, Muecksch F, et al. Enhanced SARS-CoV-2 neutralization by dimeric IgA. *Sci Transl Med* 2021;13(577):eabf1555.
47. Park JH, Lee HK. Delivery Routes for COVID-19 Vaccines. *Vaccines (Basel)* 2021;9(5):524.
48. Du Y, Xu Y, Feng J, et al. Intranasal administration of a recombinant RBD vaccine induced protective immunity against SARS-CoV-2 in mouse. *Vaccine* 2021;39:2280–7.
49. Al-Halifa S, Gauthier L, Arpin D, et al. Nanoparticle-based vaccines against respiratory viruses. *Front Immunol* 2019;10:22.
50. Schneider CS, Xu Q, Boylan NJ, et al. Nanoparticles that do not adhere to mucus provide uniform and long-lasting drug delivery to airways following inhalation. *Sci Adv* 2017;3:e1601556.
51. Shin H, Iwasaki A. A vaccine strategy that protects against genital herpes by establishing local memory T cells. *Nature* 2012;491:463–7.
52. Wu B, Zhang H, Wang YC, et al. Sequencing on an imported case in China of COVID-19 Delta variant emerging from India in a cargo ship in Zhoushan, China. *J Med Virol*. 2021;93:6828–32.
53. Liu Y, Liu J, Xia H, et al. Neutralizing activity of BNT162b2-elicited serum. *N Engl J Med* 2021;384:1466–8.
54. Liu Y, Liu Y, Xia H, et al. BNT162b2-elicited neutralization of B.1.617 and other SARS-CoV-2 variants. *Nature* 2021;596:273–5.
55. Kim HW, Canchola JG, Brandt CD, et al. Respiratory syncytial virus disease in infants despite prior administration of antigenic inactivated vaccine. *Am J Epidemiol* 1969;89:422–34.
56. Mahmoodpoor A, Sanaie S, Samadi P, et al. SARS-CoV-2: unique challenges of the virus and vaccines. *Immunol Invest* 2021;50(7):802–9.
57. Grunau B, Goldfarb DM, Asamoah-Boaheng M, et al. Immunogenicity of extended mRNA SARS-CoV-2 vaccine dosing intervals. *JAMA* 2022;327:279–81.
58. Voysey M, Costa Clemens SA, Madhi SA, et al. Single-dose administration and the influence of the timing of the booster dose on immunogenicity and efficacy of ChAdOx1 nCoV-19 (AZD1222) vaccine: a pooled analysis of four randomised trials. *Lancet* 2021;397:881–91.
59. Chen RE, Zhang X, Case JB, et al. Resistance of SARS-CoV-2 variants to neutralization by monoclonal and serum-derived polyclonal antibodies. *Nat Med* 2021;27:717–26.
60. Zou J, Xia H, Xie X, et al. Neutralization against omicron SARS-CoV-2 from previous non-omicron infection. *Nat Commun* 2022;13:852.
61. Ku Z, Xie X, Hinton PR, et al. Nasal delivery of an IgM offers broad protection from SARS-CoV-2 variants. *Nature* 2021;595:718–23.
62. Chan JF, Zhang AJ, Yuan S, et al. Simulation of the clinical and pathological manifestations of coronavirus disease 2019 (COVID-19) in a Golden Syrian Hamster Model: implications for disease pathogenesis and transmissibility. *Clin Infect Dis* 2020;71:2428–46.